HHS Public Access

Author manuscript

Neuroimage. Author manuscript; available in PMC 2020 May 01.

Published in final edited form as:

Neuroimage. 2019 May 01; 191: 325–336. doi:10.1016/j.neuroimage.2019.02.036.

Age-related alterations in axonal microstructure in the corpus callosum measured by high-gradient diffusion MRI

Qiuyun Fan[a,b,*], **Qiyuan Tian**[a,b], **Ned A. Ohringer**[a,b], **Aapo Nummenmaa**[a,b], **Thomas Witzel**[a,b], **Sean M. Tobyne**[b,c], **Eric C. Klawiter**[b,c], **Choukri Mekkaoui**[a,b], **Bruce R. Rosen**[a,b,d], **Lawrence L. Wald**[a,b,d], **David H. Salat**[a,b], and **Susie Y. Huang**[a,b,d]

[a]Athinoula A. Martinos Center for Biomedical Imaging, Department of Radiology, Massachusetts General Hospital, Charlestown, MA, USA

[b]Harvard Medical School Boston, MA, USA

[c]Department of Neurology, Massachusetts General Hospital, Boston, MA, USA

[d]Harvard-MIT Division of Health Sciences and Technology, Massachusetts Institute of Technology, Cambridge, MA, USA

Abstract

Cerebral white matter exhibits age-related degenerative changes during the course of normal aging, including decreases in axon density and alterations in axonal structure. Noninvasive approaches to measure these microstructural alterations throughout the lifespan would be invaluable for understanding the substrate and regional variability of age-related white matter degeneration. Recent advances in diffusion magnetic resonance imaging (MRI) have leveraged high gradient strengths to increase sensitivity toward axonal size and density in the living human brain. Here, we examined the relationship between age and indices of axon diameter and packing density using high-gradient strength diffusion MRI in 36 healthy adults (aged 22–72) in well-defined central white matter tracts in the brain. A recently validated method for inferring the effective axonal compartment size and packing density from diffusion MRI measurements acquired with 300 mT/m maximum gradient strength was applied to the *in vivo* human brain to obtain indices of axon diameter and density in the corpus callosum, its sub-regions, and adjacent anterior and posterior fibers in the forceps minor and forceps major. The relationships between the axonal metrics, corpus callosum area and regional gray matter volume were also explored. Results revealed a significant increase in axon diameter index with advancing age in the whole corpus callosum. Similar analyses in sub-regions of the corpus callosum showed that age-related alterations in axon diameter index and axon density were most pronounced in the genu of the corpus callosum and relatively absent in the splenium, in keeping with findings from previous histological studies. The significance of these correlations was mirrored in the forceps minor and forceps major, consistent with previously reported decreases in FA in the forceps minor but not in the forceps major with age. Alterations in the axonal imaging metrics paralleled decreases in

[*]Corresponding author. Athinoula A. Martinos Center for Biomedical Imaging, Department of Radiology, Massachusetts General Hospital, 149 Thirteenth Street, Suite 2301, Charlestown, MA, 02129, USA., qiuyun.fan@mgh.harvard.edu (Q. Fan).

Appendix A. Supplementary data

Supplementary data to this article can be found online at https://doi.org/10.1016/j.neuroimage.2019.02.036.

corpus callosum area and regional gray matter volume with age. Among older adults, results from cognitive testing suggested an association between larger effective compartment size in the corpus callosum, particularly within the genu of the corpus callosum, and lower scores on the Montreal Cognitive Assessment, largely driven by deficits in short-term memory. The current study suggests that high-gradient diffusion MRI may be sensitive to the axonal substrate of age-related white matter degeneration reflected in traditional DTI metrics and provides further evidence for regionally selective alterations in white matter microstructure with advancing age.

Keywords

Aging; Diffusion MRI; Tissue microstructure; Axon diameter; White matter; High b-value; Human connectome scanner; Human connectome project (HCP)

1. Introduction

Alterations in fiber composition within the corpus callosum, the major commissure connecting the cerebral hemispheres, interfere with the efficiency of interhemispheric transfer in older adults and likely contribute to specific patterns of cognitive aging (Janowsky et al., 1996; Jeeves and Moes, 1996). Structural changes in the corpus callosum with aging are thought to reflect changes in the functional integrity of interhemispheric processing (Schulte et al., 2005; Sullivan and Pfefferbaum, 2006; van der Knaap and van der Ham, 2011). Postmortem studies have revealed age-related changes in axon size and number in the corpus callosum, with a higher number of large myelinated callosal fibers > 1 μm observed with increasing age (Aboitiz et al., 1996). Histological analyses of different callosal segments suggest that the less myelinated fibers of the genu are particularly susceptible to the deleterious effects of aging (Aboitiz et al., 1992b; Kemper, 1994).

Noninvasive approaches to infer axon size and density in the living human brain would be invaluable for understanding the microstructural substrate of age-related degeneration of cerebral white matter. The trends in callosal fiber composition identified on histology are supported by multiple neuroimaging studies that have used diffusion magnetic resonance imaging (MRI) to infer white matter microstructural properties in the aging human brain (Abe et al., 2002; Bender et al., 2016b; Bennett and Madden, 2014; Berman et al., 2018; Bhagat and Beaulieu, 2004; Billiet et al., 2015; Branzoli et al., 2016; Chad et al., 2018; Cox et al., 2016; de Lange et al., 2016; Fjell et al., 2016, 2017; Head et al., 2004; Hsu et al., 2008; Lebel et al., 2010; Liu et al., 2018; Madden et al., 2004; Martensson et al., 2018; Moseley, 2002; Nusbaum et al., 2001; Ota et al., 2006; Pfefferbaum et al., 2000, 2005; Salat et al., 2005; Serbruyns et al., 2015; Sexton et al., 2014; Storsve et al., 2016; Stricker et al., 2015; Sullivan et al., 2001, 2006; Sullivan and Pfefferbaum, 2006; Wang et al., 2018; Xie et al., 2016; Yeatman et al., 2014). One of the most enduring findings from diffusion tensor imaging (DTI) studies across the lifespan is the regionally selective distribution of low fractional anisotropy (FA) in frontal white matter with increasing age (Bennett and Madden, 2014; Bhagat and Beaulieu, 2004; Cox et al., 2016; Head et al., 2004; Madden et al., 2012; Pfefferbaum et al., 2005; Rojkova et al., 2016; Salat et al., 2005; Sexton et al., 2014; Sullivan et al., 2006; Vik et al., 2015; Zhang et al., 2010), a finding thathas been

corroborated in non-human primates (Kubicki et al., 2018; Makris et al., 2007). An anterior-to-posterior gradient of fiber integrity, in which anterior fiber bundles are more susceptible to age-related degeneration than posterior fibers, has also been demonstrated in the corpus callosum using a variety of analytic approaches, including region-of-interest (ROI) analysis (Bender et al., 2016b; Madden et al., 2012; O'Sullivan et al., 2001; Pfefferbaum et al., 2005; Pfefferbaum and Sullivan, 2003; Salat et al., 2005; Sexton et al., 2014; Xie et al., 2016), voxel-based approaches (Hsu et al., 2008; Salat et al., 2005; Sexton et al., 2014; Zhang et al., 2010), and tract-based analyses (Bennett et al., 2010; Burzynska et al., 2010; Davis et al., 2009; Fjell et al., 2017; Lebel et al., 2012; Liu et al., 2018; Sala et al., 2012; Sullivan et al., 2001, 2006, 2010).

While DTI offers some insight into the structural integrity of white matter, conventional DTI metrics are not specific to white matter tissue properties such as myelination or fiber density, which limits the interpretation of these metrics in relation to the histological substrate of white matter degeneration. A number of advanced diffusion MRI techniques such as AxCaliber (Assaf et al., 2008; Barazany et al., 2009), three-dimensional AxCaliber (Amitay et al., 2016) and ActiveAx (Alexander et al., 2010) have been developed in an attempt to quantify restricted diffusion within axons using simplified, geometric models of axons as impermeable cylinders of finite diameter and packing density. More recent theoretical and experimental work has shown that the parameters approximated by such simplified white matter models may capture neural substrates beyond the intra-axonal space, including diffusion within the extra-axonal space demonstrating a high degree of effective restriction (Burcaw et al., 2015; Fieremans et al., 2016; Lee et al., 2018). Acknowledging the ongoing debate regarding the interpretation of such axonal imaging metrics, we refer to the estimates derived by such models as the size and packing density of the restricted cylindrical diffusion compartment (i.e., cylinder diameter and packing density), which may then be interpreted as an index of axon diameter and packing density.

Despite the caveats regarding the interpretation of the derived metrics, advanced microstructural models of diffusion within white matter have become more readily translated to studying the *in vivo* human brain, largely through the availability of higher gradient strengths on human MRI scanners (Fan et al., 2014; Setsompop et al., 2013). Higher gradient strengths push the diffusion resolution limit to approach the length scale of axons and cells, with measurements using gradient strengths up to 300mT/m becoming sensitive to intra- and extra-axonal diffusion (Huang et al., 2015b; McNab et al., 2013). Such technological advancements offer the possibility of inferring trends in effective axonal compartment size and packing density in the living human brain and serving as a window into the axonal alterations that occur during the course of normal aging.

The goal of the current work is to study the age-related trajectories of an index of axon diameter and packing density as estimated from high-gradient diffusion MRI in the midline corpus callosum and to determine whether alterations in these metrics correlate with other measures of white and gray matter degeneration with age. We examine whether such differences demonstrate a regional selectivity that might provide insight into the axonal changes that occur with advancing age. If present, axonal alterations would be expected to be most pronounced in the genu of the corpus callosum compared to other callosal segments,

with a projected increase in the axon diameter index with age based on previously reported findings from histology. A secondary aim is to examine whether age-related axonal alterations are associated with changes in DTI metrics in the corpus callosum and contiguous anterior (*i.e.*, forceps minor) and posterior (*i.e.*, forceps major) white matter tracts, as well as connected gray and white matter areas, which would lend support to the anterior-to-posterior gradient hypothesis of age-related white matter degeneration.

To achieve these goals, we examine the trends in axon diameter index and packing density estimated from high-gradient diffusion MRI in the corpus callosum and its sub-regions in a cross-sectional study of healthy adults across the lifespan. We apply a previously validated multidiffusion time, multi-gradient strength diffusion MRI acquisition using gradient strengths ranging up to 300 mT/m to recover estimates of the axon diameter index and packing density in the midline corpus callosum, forceps major, and forceps minor and compare the strength of the associations between the microstructural metrics and age in each tract. We also investigate the relationship between the axonal imaging metrics in the corpus callosum and age-related cognitive differences in an effort to place these metrics in context with other imaging-based biomarkers and demonstrate the potential utility of such metrics in future studies of white matter degeneration in aging.

2. Methods

2.1 Participants

A total of 36 healthy, cognitively normal adults between the ages of 22 and 72 (23 women, 13 men) were recruited through the Massachusetts General Hospital and local community with approval from the institutional review board. All participants provided written informed consent. Each participant was screened to ensure that he or she was in good health and cognitively intact with no history of major metabolic, neurologic or psychiatric conditions, including dementia, cerebrovascular disease, brain tumors, major head trauma, and other neurologic and psychiatric conditions that could influence cognition or imaging measures. In addition, all older participants aged ≥ 50 years underwent further screening for cognitive impairment using the Montreal Cognitive Assessment (MoCA) (Nasreddine et al., 2005), revealing scores within the normal range (≥26), with a mean score of 28.9 ± 0.94. Twenty-five participants were Caucasian, seven were Asian, three were African-American, and one was Hispanic.

2.2 Data acquisition

All participants underwent MRI on a dedicated 3T MRI scanner equipped with maximum gradient strength of 300 mT/m (Magnetom Skyra CONNECTOM, Siemens Healthineers, Erlangen, Germany) (Fan et al., 2016; McNab et al., 2013; Setsompop et al., 2013) using a custom-made 64-channel phased array head coil (Keil et al., 2013) for signal reception. The diffusion MRI protocol consisted of a multi-diffusion time, multi-gradient strength acquisition with whole brain coverage using a single-refocused monopolar Stejskal-Tanner pulsed gradient spin-echo, echo planar imaging (EPI) sequence (TR/TE = 4000/77 ms, simultaneous multi-slice (SMS) (Feinberg et al., 2010; Feinberg and Setsompop, 2013; Setsompop et al., 2012a, 2012b) acceleration factor of 2, in-plane acceleration using

Generalized Autocalibrating Partially Parallel Acquisition (GRAPPA) (Griswold et al., 2002) with an acceleration factor of 2, partial Fourier 6/8, voxel size 2 × 2 × 2 mm, anterior-to-posterior phase-encoding direction). The imaging protocol was modeled after an AxCaliber-type acquisition that incorporated angular sampling as previously described (Fan et al., 2018; Huang et al., 2015a) using a fixed diffusion gradient pulse duration δ = 8 ms, two diffusion times (Δ = 19 and 49 ms) and eight linearly spaced gradient strengths (G) ranging from 26 to 290 mT/m per diffusion time, with 32 or 64 diffusion encoding directions sampled per gradient strength, as specified in Table 1, and $b = 0 s/mm^2$ images interspersed every 16 diffusion-weighted volumes for motion correction. The number of diffusion directions was chosen based on b-value, with 32 directions used for $b \leq 2300$ s/mm^2 and 64 directions for $b \geq 2400$ s/mm^2. In addition, five $b = 0$ images with reversed (i.e., posterior-to-anterior) phase-encoding direction were acquired to correct for susceptibility-induced image distortion.

Diffusion MRI acquisition parameters including diffusion time (Δ), diffusion gradient pulse duration (δ), b-values and number of diffusionencoding gradient directions.

T_1-weighted structural images with 1-mm isotropic voxel size were acquired for all subjects using a multi-echo magnetization-prepared gradient echo (MEMPRAGE) sequence (van der Kouwe et al., 2008) (TR/TE = 2530/1.15 ms, GRAPPA = 3, inversion time TI = 1100 ms, and flip angle = 7°).

2.3 Data analysis

The diffusion MRI data were processed and analyzed following an established pipeline with the following steps: (1) preprocessing to correct for motion, eddy current and susceptibility-induced distortions; (2) fitting of the corrected multi-diffusion time, multi-gradient strength data to obtain estimates of cylinder diameter, restricted volume fraction, and packing density; (3) calculation of FA and mean diffusivity (MD) maps from the $b = 950$ s/mm^2 data; (4) quantification of diffusion MRI metrics in the whole corpus callosum and its sub-divisions based on segmentation of the corpus callosum using FreeSurfer software; and (5) quantification of diffusion MRI metrics in selected tracts other than the corpus callosum using regions of interest derived from the Johns Hopkins University (JHU) white matter tractography atlas. Each of these steps is described in detail below.

2.3.1 Data preprocessing—To process the diffusion MRI data, we used the data preprocessing pipeline established for the MGH-USC Human Connectome Project (Fan et al., 2016) as well as tools available as part of the FreeSurfer (Fischl, 2012) (http://surfer.nmr.mgh.harvard.edu) and FMRIB Software Library (Smith et al., 2004) (FSL, https://fsl.fmrib.ox.ac.uk) processing streams. All MR images were corrected for gradient nonlinearity using in-house Matlab code. The diffusion MRI data was corrected for motion as well as susceptibility- and eddy current-induced distortions using the TOPUP (Andersson et al., 2003) and EDDY functions (Andersson and Sotir- opoulos, 2016; Andersson et al., 2016) included in FSL.

2.3.2 Fitting for diffusion MRI metrics—Estimates of cylinder diameter, restricted and cerebrospinal fluid (CSF) volume fraction, and hindered diffusivity were obtained by

fitting the corrected multi-diffusion time, multi-gradient strength diffusion MRI data to a validated three-compartment model of intra-axonal restricted diffusion, extra-axonal hindered diffusion, and free diffusion (Fan et al., 2018). Briefly, generalized *q*-sampling imaging (Yeh et al., 2010) was first used to identify the principal fiber direction in each voxel by searching for the global maximum on the orientation distribution function of diffusing spins using the $\Delta = 19$ ms diffusion MRI data. The signal was then resampled for each diffusion-encoding direction and was averaged along the equator about the principal fiber direction to obtain the mean perpendicular signal using a Gaussian weighting function dependent on the distance of each resampling vertex from the equator (Fan et al., 2018; Tuch, 2004). The aforementioned three-compartment model was fitted to this mean perpendicular signal to derive estimates of the cylinder diameter, restricted volume fraction, CSF volume fraction, and hindered diffusivity. Intra-axonal diffusion was modeled by restricted diffusion in impermeable parallel cylinders following the van Gelderen model (van Gelderen et al., 1994), which uses the Gaussian phase distribution approximation to account for diffusion during the diffusion-encoding gradient pulse. Gaussian diffusion was assumed for hindered diffusion in the extra-axonal space, and free water diffusion was assumed for the CSF compartment.

Model fitting was performed on a voxel-wise basis using Markov chain Monte Carlo (MCMC) sampling. MCMC simulations provided samples of the posterior distributions of the model parameters given the data. Broad uniform priors with the ranges given in parentheses were used for cylinder diameter (0.1–20 μm), restricted volume fraction (0–1), CSF volume fraction (0–1), and hindered diffusivity (0.1–2 $\mu m^2/ms$). The restricted diffusion coefficient D_r was set to 1.7 $\mu m^2/ms$, which is comparable to the estimated *in vivo* axial diffusivity in white matter and in keeping with values used in prior studies (Alexander et al., 2010; Huang et al., 2015b). The diffusion coefficient of CSF was assumed to be that of free water at 37 °C (3 $\mu m^2/ms$). A Rician noise model was adopted for parameter estimation (Alexander, 2008; Alexander et al., 2010). The total number of MCMC samples calculated for each voxel was 1,800. MCMC samples were saved at intervals of 100 iterations after an initial burn-in period of 20,000 iterations. The mean estimates for cylinder diameter, restricted and CSF volume fractions, and hindered diffusivity were then calculated for each voxel by taking the mean over the MCMC samples. The packing density was calculated by weighting the restricted fraction by the cross-sectional area calculated using the mean cylinder diameter, as described previously (Alexander et al., 2010; Huang et al., 2016).

White matter tract integrity (WMTI) (Fieremans et al., 2011) and Neurite Orientation Dispersion and Density Imaging (NODDI) analyses were performed to corroborate the derived axonal metrics. Specifically, the WMTI analysis was performed using the diffusion kurtosis imaging software package () with all diffusion MRI data acquired with a *b*-value < 3000 s/mm^2 (Jensen and Helpern, 2010), and NODDI analysis was performed using two shells ($b = 950$ s/mm^2, 32 directions and $b = 2400$ s/mm^2, 64 directions) matched to the optimal *in vivo* human protocol (Zhang et al., 2012).

DTI metrics of fractional anisotropy (FA), mean diffusivity (MD), radial diffusivity (RD), and axial diffusivity (AD) were calculated using a least-squares fit to the diffusion MRI data

acquired at $b = 950$ s/mm^2 with a diffusion time of 49 ms and 32 diffusion-encoding gradient directions.

2.3.3 Regional analysis in the corpus callosum—A standard FreeSurfer reconstruction (version 6.0) was performed using the T_1-weighted MEMPRAGE images for each subject to achieve automatic subcortical segmentation and voxel-wise labeling of the brain (Dale et al., 1999; Fischl et al., 1999). A whole brain white matter mask was created from the FreeSurfer labels for the right and left cerebral hemispheric white matter. A corpus callosum mask on three mid-sagittal slices was created from the FreeSurfer labels and manually edited to ensure exclusion of voxels outside the corpus callosum (e.g., fornix and CSF). The corpus callosum was further divided into five sub-sections (anterior, mid-anterior, central, mid-posterior, and posterior) using FreeSurfer's automatic labeling with the mri_cc command to delineate callosal segments (Fischl et al., 2002). The five sub-sections were derived from evenly spaced partitions along the primary eigenaxis, closely corresponding to the longitudinal axis (Fig. 1).

The average of the interleaved $b = 0$ images after susceptibility correction was registered to the T_1-weighted MEMPRAGE image using the boundary-based registration tool in FreeSurfer with 6 degrees of freedom, and the FreeSurfer labels in native T_1-weighted image space were transformed into diffusion image space using the inverse of the diffusion-to-T_1-weighted image transformation.

The whole brain white matter and corpus callosum masks were refined to include voxels with minimal partial volume effects with gray matter or CSF by excluding voxels with low FA values. For the whole brain white matter mask, we chose to threshold FA at 0.2, as in (Salat et al., 2005). For the corpus callosum mask, we used a slightly higher value of 0.4 to threshold FA, due to the expected higher packing density and orientational coherence of the fibers in that structure. Note that the results were not significantly altered with the application of these different thresholds, suggesting that partial volume effects were not a major determinant of the results. The higher end of these thresholds was conservative as the FA of CSF and gray matter is typically below 0.2 and 0.4, respectively.

Corpus callosum area as well as corpus callosum area normalized to total intracranial volume were also measured, following the approach outlined in Tobyne et al. (2016).

2.3.4 Regional analysis in the forceps major/minor—To quantify diffusion MRI metrics in the tracts extending from the anterior (genu) and posterior (splenium) portions of the corpus callosum, the Johns Hopkins University (JHU) white matter probabilistic tractography atlas (Mori et al., 2008) was used to create regions of interest (ROIs) for the forceps minor and forceps major in each participant's native diffusion space. These two tracts were selected because the axonal fibers are largely aligned in a coherent orientation, so that a single primary fiber orientation can be assumed. The FA map of each participant was first linearly registered to the template FA map in the JHU atlas using NiftyReg's "reg_aladin" function (https://cmiclab.cs.ucl.ac.uk/mmodat/niftyreg). The linearly transformed FA map was then non-linearly registered to the template FA map using NiftyReg's "reg_f3d" function. The transformation was inverted to transform the

probabilistic tractography maps (thresholded at 25%) of the forceps major and forceps minor from atlas space to each subject's native diffusion space to define the ROIs for these white matter tracts. Voxels with FA values below 0.2 were excluded, similar to the procedure described above for the corpus callosum.

2.3.5 Regional analysis with gray matter volumes—The FreeSurfer automatic pipeline was used to segment the cerebral cortex into seven lobules, including prefrontal, frontal, central, parietal, occipital, temporal and cingulate regions (Fig. 2), by regrouping the smaller segments in the Destrieux atlas (Fischl et al., 2004). The gray matter volumes for prefrontal cortex and the parietal and occipital cortices combined were extracted, which were then divided by the total intracranial volume to obtain normalized regional gray matter volumes. Correlation analyses were performed between the axonal metrics in the genu and the normalized prefrontal cortical volumes, and between the axonal metrics in the splenium and the normalized gray matter volume of the parietal and occipital cortices combined. The correlation analyses were performed for genu and splenium of the corpus callosum to explore the anterior-posterior gradient of age-related white matter alterations. The prefrontal, parietal and occipital cortices were selected, because they are identified as dominantly connected with genu and splenium, respectively (Hofer and Frahm, 2006).

2.3.6 Statistical analyses—We examined the ROI-averaged data using Pearson's correlation among all participants. Correction for multiple comparisons based on the false discovery rate (FDR) with an FDR threshold of 0.05 was applied to account for multiple comparisons. The raw uncorrected *p*-values surviving FDR correction are reported here.

3. Results

3.1 Whole corpus callosum analysis

Voxel-wise estimates of the axon diameter index, restricted volume fraction, and packing density were obtained for the midline corpus callosum (Fig. 3). Fig. 4 presents scatterplots for correlations between age and the axonal imaging metrics in the whole corpus callosum. These analyses showed a significant increase in the axon diameter index ($r = 0.42$, $p = 0.01$) and reduction in packing density ($r = —0.41$, $p = 0.01$) with increasing age throughout the corpus callosum. By comparison, no significant correlation was observed between FA and age in the whole corpus callosum, although a significant reduction in FA was observed with increasing age globally in the cerebral white matter, in agreement with previous reports (Salat et al., 2005). Significant reductions in callosal area ($r = —0.52$, $p = 0.001$) and callosal area normalized to total intracranial volume ($r = —0.45$, $p = 0.005$) were observed with increasing age. The correlations described above remained significant after controlling for gender (Table 2). No significant correlation with age was found for the WMTI or NODDI metrics in the whole corpus callosum after FDR correction for multiple comparisons (Fig. S1). The fiber orientation dispersion was fairly low at the callosal midline (around or below 0.1, Figs. S1-6), as expected from previous studies (Mollink et al., 2017).

3.2 Regional analyses in the corpus callosum

Diffusion MRI estimates of the axon diameter index and packing density were regionally variable in the corpus callosum. Scatterplots for the correlations between age, axon diameter index and packing density in each corpus callosum segment are presented in Fig. 5. These analyses showed a statistically significant increase in the axon diameter index with increasing age in the genu ($r = 0.48$, $p = 0.01$) and a significant reduction in axon density in the genu ($r = —0.57$, $p < 0.001$) and posterior body ($r = —0.48$, $p = 0.003$) of the corpus callosum. The correlations between age and the axonal imaging metrics of diameter and packing density were significantly stronger in the genu of the corpus callosum than in the splenium (see Table S1 in the Supplementary Material for a detailed description of the statistical comparison). No significant correlation was observed between age and restricted volume fraction in any corpus callosum segment. The WMTI metrics showed the strongest age-related effects in the genu relative to the other callosal segments (Table S1), with a significant decrease in axonal water fraction ($r = —0.46$, $p = 0.005$) and increase in extra-axonal radial diffusivity ($r = 0.48$, $p = 0.003$) observed with increasing age (Fig. S2). No significant correlation with age was found between the NODDI metrics in the five segments of the corpus callosum (Figs. S2-S6). FA was only significantly correlated with age in the genu of the corpus callosum ($r = —0.38$, $p = 0.02$) and not in the other segments.

Scatterplots demonstrating the relationship between the DTI metrics of FA, MD, RD and AD and the axonal microstructural metrics of axon diameter index, restricted volume fraction, and packing density in the corpus callosum are presented in Fig. 6. The scatterplots were generated using the DTI metrics and axonal metrics for the corpus callosum regions defined in Fig. 1 in all subjects. No significant correlation was observed between axon diameter index and DTI metrics including FA, AD, RD and MD. On the other hand, a strong positive correlation was identified between restricted volume fraction and FA and RD, and a moderate correlation was appreciated between packing density and the DTI metrics of FA, RD and AD. The strength of the correlations was preserved after controlling for age, indicating that the relationship between axonal metrics (i.e., restricted volume fraction and packing density) and DTI metrics (i.e., FA, RD and AD) captured a relationship beyond what age effects could explain. Of all the DTI metrics, FA showed the strongest correlations with restricted volume fraction and packing density. We thus chose to focus our comparisons of the axonal metrics with the DTI metric of FA in subsequent analyses

3.3. Regional analyses in the forceps major and minor

Regional analyses of the relationships between age and axonal metrics in the forceps minor and forceps major supported the anterior-to-posterior trend observed in the corpus callosum ROI analyses (Fig. 7). Specifically, in the forceps minor, the major white matter bundle that connects the frontal lobes via the genu of the corpus callosum, the axon diameter index significantly increased with age ($r = 0.48$,$p = 0.003$), and the packing density decreased with age ($r = —0.40$, $p = 0.01$). By comparison, in the forceps major, which connects the occipital lobes via the splenium of the corpus callosum, no significant correlation was seen between age and axon diameter index or packing density. FA was significantly correlated with age in the forceps minor ($r = —0.62$, $p < 0.0001$) and not in the forceps major.

3.4 Association of axonal metrics with regional gray matter volume

For the genu of the corpus callosum, a significant negative correlation was found between the normalized gray matter volume of the prefrontal region and axon diameter index ($r = —0.41$, $p = 0.013$), and a positive correlation was found with estimated packing density ($r = 0.56$, $p < 0.001$). The significance of these relationships was maintained when adjusting for FA, with lower normalized gray matter volume in the prefrontal region correlating with larger effective axonal compartment size ($r =—0.40$, $p = 0.016$) and decreased packing density ($r = 0.43$, $p = 0.008$). No significant correlation was found between the splenium axonal metrics and the parietal and occipital volume (Fig. 8).

3.5 Relationship of axonal metrics with cognition

Among the 10 older adults who underwent MoCA testing, there was a borderline significant association between MoCA score and age ($r = 0.628$, $p = 0.05$). A similar strength of association was observed between MoCA scores and imaging markers in the whole corpus callosum adjusted for age, including axon diameter index ($r = —0.629$, $p = 0.10$), restricted volume fraction ($r =—0.638$, $p = 0.16$), packing density ($r = —0.628$, $p = 0.17$), FA ($r = —0.630$,$p = 0.17$), and normalized corpus callosum area ($r = 0.632$, $p = 0.16$). Among the sub-regions of the corpus callosum, larger axon diameter index in the genu of the corpus callosum was significantly correlated with lower MoCA score adjusted for age ($r =—0.843$, $p = 0.01$), with the subscore for short-term memory showing the strongest correlation with axon diameter index in the genu ($r = —0.717$, $p = 0.07$) and not in the other segments. No significant association was observed between MoCA scores and restricted volume fraction, packing density, or FA for sub-regions of the corpus callosum.

4. Discussion

In this study, we observed regionally selective, age-related differences in axon diameter index and density in the corpus callosum and adjacent white matter tracts estimated from high-gradient diffusion MRI. A global increase in axon diameter index and decrease in packing density was seen throughout the corpus callosum with increasing age, with the effect being most pronounced in the genu of the corpus callosum. The findings were mirrored by similar trends in the adjacent forceps minor and forceps major, with the forceps minor demonstrating a significant increase in axon diameter index and decrease in packing density, consistent with alterations seen in the genu, but not observed in the forceps major or splenium. Our results support the hypothesis that select fiber bundles are preferentially affected by aging, and that these trends follow a regional distribution that reflects the selective vulnerability of certain anterior fiber bundles to age-related degeneration. More importantly, the axonal imaging metrics provide unique and complementary regional markers of microstructural changes relative to DTI. This approach offers a more specific microstructural interpretation of the axonal changes underpinning the previously noted age-related differences in FA within anterior versus posterior fiber bundles, suggesting that the underlying substrate of age-related degeneration may relate to fiber size and packing density.

Our results are in agreement with previous histological studies demonstrating an age-related increase in axon diameter and overall decrease in density of myelinated fibers in the human

corpus callosum (Aboitiz et al., 1996; Marner et al., 2003). In a postmortem study of 20 individuals aged 25–68 years who died from non-neurologic causes, the numbers of medium and large callosal fibers consistently increased in the genu of the corpus callosum in both males and females (Aboitiz et al., 1996). The age-related correlations reported here and in prior histological studies of the corpus callosum did not affect the relative estimates of axon diameter index or packing density along the corpus callosum, which maintained the same low-high-low pattern of axon diameter and high-low-high distribution of axon density from anterior-to-posterior throughout the lifespan (Aboitiz et al., 1992a, 1996). Our findings support the hypothesis that callosal fibers may increase in size with age, particularly in the anterior callosum, resulting in an overall increase in the numbers of larger diameter fibers at the expense of smaller diameter fibers. It has been postulated that the functional significance of a shift toward larger diameter myelinated fibers with age may be to compensate for decreasing interhemispheric transfer efficiency in older adults by recruiting faster conducting fibers (Reuter-Lorenz and Stanczak, 2000).

The current work provides insight into the microstructural substrate of white matter degeneration with aging and represents a potential link between the imaging and histological domains that requires further validation. Previous diffusion imaging studies of regional FA in the corpus callosum reported an anterior to posterior gradient, with FA in the genu and rostral body exhibiting the greatest decline with advancing age and FA in the splenium remaining relatively stable (Bender et al., 2016b; Bennett et al., 2010; Burzynska et al., 2010; Madden et al., 2012; Ota et al., 2006; Pfefferbaum et al., 2005; Salat et al., 2005; Sexton et al., 2014; Zhang et al., 2010). Quantitative fiber tracking approaches have revealed similar trends in the corpus callosum, with disproportionately lower FA in anterior fiber bundles relative to posterior bundles in older adults compared to younger adults (Bender et al., 2016b; Bennett et al., 2010; Burzynska et al., 2010; Davis et al., 2009; Lebel et al., 2012; Sullivan et al., 2006, 2010; Xie et al., 2016). Other neuroimaging studies have demonstrated that the prefrontal cortex and prefrontal white matter are associated with numerous age-related changes, including accelerated cortical atrophy and white matter volume loss (Lebel et al., 2012; Raz et al., 2004). Age-related decreases in FA are consistently greater in the frontal white matter compared to the temporal, parietal and occipital white matter (Bender et al., 2016b; Bennett and Madden, 2014; Cox et al., 2016; Head et al., 2004; Madden et al., 2012; Salat et al., 2005; Sexton et al., 2014; Vik et al., 2015), a finding that is supported by the presently reported increase in axon diameter index and decrease in packing density with age in the forceps minor but not the forceps major.

A number of advanced diffusion imaging approaches have emerged in recent years that offer greater specificity and insight into the types of white matter microstructural alterations that occur in non-pathological brain aging. In the current work, we applied a generalized approach to fit for axon diameter index and density and compared our results with DTI-derived parameters. The axon diameter index did not correlate with any of the DTI metrics, suggesting that the effective compartment size inferred by our approach may be independent of and complementary to the microstructural properties captured by DTI. On the other hand, restricted volume fraction and packing density showed relatively strong correlations with FA, RD, and to a lesser degree, AD. Of all the DTI metrics, FA showed the strongest correlations with restricted volume fraction and packing density. While we acknowledge the

well-known association of increasing MD with age, recent work has shown that this trend can be accounted for by diffusion models that explicitly estimate the amount of free water in white matter (Chad et al., 2018), as our model does. In our analysis, we found an increase in the CSF volume fraction derived from our three-compartment model with age ($r = 0.33$, $p = 0.047$), which agrees with the known association between MD and age. The validity of the axon diameter index in the presence of altered MD is supported by our use of a three-compartment model that treats the restricted, hindered and CSF compartments separately, which largely disassociates the axon diameter index estimation from MD.

The strong correlation between FA and restricted volume fraction motivated us to study the relationship of analogous advanced diffusion imaging metrics with age, including axonal water fraction derived from WMTI and intracellular water fraction derived from NODDI. We were able to replicate the known negative correlation between age and FA in the global cerebral white matter (Salat et al., 2005), but the age effect was weak in the corpus callosum FA. Similarly, the restricted volume fraction estimated by the WMTI and NODDI approaches in the whole corpus callosum did not reveal significant age effects. By comparison, the estimate of packing density obtained by dividing the restricted volume fraction by the mean cross-sectional area showed the best correlation with age, implying that incorporating information about axon diameter index helped to demonstrate an association between packing density and age that was not readily apparent from the restricted volume fraction alone. In a sub-region analysis of WMTI and NODDI metrics in the corpus callosum, the axonal water fraction showed a significant decrease with age in the genu, consistent with our finding of decreased packing density in the genu. Although the results of WMTI, NODDI and our approach cannot be compared directly, the consistent results obtained by these various models suggests that advanced diffusion models can provide greater specificity to the axonal alterations that occur in aging compared to DTI.

Another well-known effect of normal aging is brain atrophy in both cerebral white matter (Gunning-Dixon et al., 2009) and gray matter (Fjell et al., 2009). Previous studies have suggested that alterations in white matter integrity as assessed by DTI correlate with and may predict regional white matter volume loss (Draganski et al., 2011; Salat et al., 2005). In our study, there was a trend toward larger diameter of the restricted cylindrical compartment with decreasing normalized corpus callosum area (see Supplementary Material). This is not a surprising finding since both variables are correlated with age. However, it might be worth note that the relationship was similar after adjusting for FA, suggesting that the metrics provided by the advanced diffusion model employed in this study might be able to capture additional information regarding axonal microstructure and its contribution to white matter degeneration beyond what a tensor model could provide. Prior studies have shown that age-related white matter microstructural changes as detected by DTI parallel and possibly precede regional gray matter volume loss (Draganski et al., 2011; Giorgio et al., 2010). To examine the potential contribution of the axonal imaging metrics toward understanding how axonal degeneration and gray matter atrophy with aging are coupled, we analyzed the relationship of the axonal metrics in the corpus callosum and regional cortical volume. A decrease in gray matter volume in the prefrontal region was significantly correlated with decreased packing density in the genu of the corpus callosum, accompanied by an observed increase in the axon diameter index. The significance of these relationships was maintained

after adjusting for FA. On the other hand, no significant correlation was observed between the axonal metrics in the splenium and the gray matter volume in the parietal and occipital cortices. Taken together, these results suggest that alterations in packing density and axon diameter index parallel regional gray matter volume loss. Defining the precise temporal evolution of axonal alterations with regional cerebral white matter and gray matter atrophy in normal aging will require further investigation in larger-scale, longitudinal studies.

Age-related white matter degeneration as measured by DTI has been shown to relate to a decline in cognitive performance in specific domains (Bender et al., 2016a), with decreased FA and increased MD in anterior white matter bundles correlating with decreased processing speed and poorer working memory (Kennedy and Raz, 2009). Our preliminary findings support an association between age and axon diameter index in the corpus callosum, particularly within the genu, and lower scores on the MoCA driven largely by deficits in short-term memory. While the sample size for this correlation analysis was small, these findings suggest that such axonal imaging metrics could provide more specific information regarding the structural substrate of cognitive differences with aging and merit further study in a larger group of subjects with more comprehensive cognitive testing across the lifespan.

The limitations of the current study are being addressed in ongoing work. Our primary analysis of axon diameter index and packing density focused on the midline corpus callosum, where the assumption of a single fiber population in each voxel is valid. Acknowledging the potential limitations of the single fiber model, we limited our ROI analysis outside of the corpus callosum to the contiguous forceps minor and forceps major, which are both unidirectional fiber bundles with high FA that largely satisfy the single fiber assumption. We have previously validated the axon diameter index estimates recovered through this analysis with similar measurements in a biomimetic brain phantom composed of parallel and crossing hollow-core textile axon fibers and shown that the restricted volume fraction estimates are more severely affected than the diameter index estimates in crossing fiber regions. To extend this work to fiber populations throughout the whole brain, future analyses will focus on fitting a generalized model that accounts for fiber orientation, compartment size, and restricted volume fraction for multiple fiber populations in each voxel. Similar approaches have been suggested by others, including the combined hindered and restricted model of water diffusion (CHARMED) (Assaf and Basser, 2005), AxCaliber 3D (Amitay et al., 2016; Barazany et al., 2011), and ActiveAx (Alexander et al., 2010).

In this work, we used a simple cylindrical model of axons to infer axonal diameter and density for callosal fibers and those in the forceps minor and forceps major. Our model resulted in overall larger diameter estimates compared to known values from histology while recovering the expected trends in axon diameters in the corpus callosum. Rather than serving as fully quantitative measures of axon diameter and density, our results may be interpreted as axon diameter- and volume fraction-weighted images that capture broad trends in axonal size and packing density, thereby enabling us to infer trends in axonal size and density with increasing age, even as the range of values reported here (~2–6 μm) are known to overestimate the majority of axon diameters in the human brain by nearly an order of magnitude. This is a well-known problem with existing approaches to axon diameter estimation using diffusion MRI and drives at a number of limitations related to diffusion

modeling and acquisition. The use of a single diameter value to summarize the average compartment size biases the estimation to larger axon diameter index. Larger axons contain more water and have a greater contribution to the overall diffusion signal decay compared to the highly restricted water within small diameter axons (Alexander et al., 2010). Furthermore, although the use of higher maximum gradient strengths has been shown to decrease estimates of axon diameter index *in vivo* (Huang et al., 2015b) and improve the contrast and stability of these estimates (Dyrby et al., 2013), axons smaller than ~3 μm remain below the diffusion resolution limit at 300mT/m (Nilsson and Alexander, 2012; Nilsson et al., 2017). Finally, the time-dependence of water diffusion in the extra-axonal space was not accounted for and could conceivably bias the estimates of diameter to larger values (Burcaw et al., 2015; De Santis et al., 2016; Fieremans et al., 2016; Novikov et al., 2014), although the range of diffusion times used in our study was relatively small (19–49 ms).

The cross-sectional design of this study of the normal aging brain supports the concept of differential aging within different segments of the corpus callosum and, by extension, different topographical regions of the brain. Nevertheless, the cross-sectional design is restricted to revealing age-related differences, not actual longitudinal changes due to possible cohort effects and uncontrolled factors that may confound true changes due to aging. Interpretation of these cross-sectional findings in a modestsized sample requires caution and merits further investigation using direct histopathological correlation in postmortem brain specimens obtained from deceased individuals across the lifespan. The modest sample size with subjects spanning a relatively large age range (50 years) and uneven age distribution with more participants in the youngest age group could conceivably limit the statistical power to detect age-related effects. Nevertheless, we were still able to detect significant correlations between the axonal metrics and age across the whole age range in certain segments of the corpus callosum, which speaks to the robustness of the age effects observed in this study. Within the limits of the current sample, study design and imaging technique, our results support the hypothesis of a preferential vulnerability of specific fibers in the corpus callosum, including the genu, and the adjacent forceps minor, with larger axon diameter index and decreased packing density reflecting age-related axonal degeneration.

Supplementary Material

Refer to Web version on PubMed Central for supplementary material.

Acknowledgments

This work was funded by a National Institutes of Health Blueprint for Neuroscience Research Grant U01MH093765 and a National Institutes of Health Brain Research through Advancing Innovative Neurotechnologies (BRAIN) Initiative Grant U01EB026996, as well as National Institutes of Health funding from the National Center for Research Resources P41EB015896, National Institute of Biomedical Imaging and Bioengineering R01EB006847 and R00EB015445, National Institute of Neurological Disorders and Stroke K23NS096056 and K23NS078044, National Heart, Lung, and Blood Institute R01HL131635 and R56HL125590, National Institute of Nursing Research R01NR010827, and Instrumentation Grants S10-RR023401, S10-RR023043, and S10-RR019307. Funding support was also received from the National Multiple Sclerosis Society, the American Heart Association Postdoctoral Fellowship Award (17POST33670452), a Radiological Society of North America Research Resident Grant (RR1427), the Conrad N. Hilton Foundation (17330) and the

Massachusetts General Hospital Executive Committee on Research Fund for Medical Discovery Fellowship Award and Claflin Distinguished Scholar Award.

References

Abe O, Aoki S, Hayashi N, Yamada H, Kunimatsu A, Mori H, Yoshikawa T, Okubo T, Ohtomo K, 2002 Normal aging in the central nervous system: quantitative MR diffusion-tensor analysis. Neurobiol. Aging 23, 433–441. [PubMed: 11959406]

Aboitiz F, Rodriguez E, Olivares R, Zaidel E, 1996 Age-related changes in fibre composition of the human corpus callosum: sex differences. Neuroreport 7, 1761–1764. [PubMed: 8905659]

Aboitiz F, Scheibel AB, Fisher RS, Zaidel E, 1992a Fiber composition of the human corpus callosum. Brain Res 598, 143–153. [PubMed: 1486477]

Aboitiz F, Scheibel AB, Zaidel E, 1992b Morphometry of the Sylvian fissure and the corpus callosum, with emphasis on sex differences. Brain 115 (Pt 5), 1521–1541. [PubMed: 1422802]

Alexander DC, 2008 A general framework for experiment design in diffusion MRI and its application in measuring direct tissue-microstructure features. Magn. Reson. Med 60, 439–448. [PubMed: 18666109]

Alexander DC, Hubbard PL, Hall MG, Moore EA, Ptito M, Parker GJ, Dyrby TB, 2010 Orientationally invariant indices of axon diameter and density from diffusion MRI. Neuroimage 52, 1374–1389. [PubMed: 20580932]

Amitay SB, Lifshits S, Barazany D, Assaf Y, 2016 3-dimensional Axon Diameter Estimation of White Matter Fiber Tracts in the Human Brain Organization for Human Brain Mapping, Geneva, Switzerland.

Andersson JL, Skare S, Ashburner J, 2003 How to correct susceptibility distortions in spin-echo echo-planar images: application to diffusion tensor imaging. Neuroimage 20, 870–888. [PubMed: 14568458]

Andersson JL, Sotiropoulos SN, 2016 An integrated approach to correction for off- resonance effects and subject movement in diffusion MR imaging. Neuroimage 125, 1063–1078. [PubMed: 26481672]

Andersson JLR, Graham MS, Zsoldos E, Sotiropoulos SN, 2016 Incorporating outlier detection and replacement into a non-parametric framework for movement and distortion correction of diffusion MR images. Neuroimage 141, 556–572. [PubMed: 27393418]

Assaf Y, Basser PJ, 2005 Composite hindered and restricted model of diffusion (CHARMED) MR imaging of the human brain. Neuroimage 27, 48–58. [PubMed: 15979342]

Assaf Y, Blumenfeld-Katzir T, Yovel Y, Basser PJ, 2008 AxCaliber: a method for measuring axon diameter distribution from diffusion MRI. Magn. Reson. Med 59, 1347–1354. [PubMed: 18506799]

Barazany D, Basser PJ, Assaf Y, 2009 In vivo measurement of axon diameter distribution in the corpus callosum of rat brain. Brain 132, 1210–1220. [PubMed: 19403788]

Barazany D, Jones DK, Assaf Y, 2011 AxCaliber 3D. In: Proceedings of the International Society of Magnetic Resonance in Medicine, p. 76.

Bender AR, Prindle JJ, Brandmaier AM, Raz N, 2016a White matter and memory in healthy adults: coupled changes over two years. Neuroimage 131, 193–204. [PubMed: 26545457]

Bender AR, Volkle MC, Raz N, 2016b Differential aging of cerebral white matter in middle-aged and older adults: a seven-year follow-up. Neuroimage 125, 74–83. [PubMed: 26481675]

Bennett IJ, Madden DJ, 2014 Disconnected aging: cerebral white matter integrity and age-related differences in cognition. Neuroscience 276, 187–205. [PubMed: 24280637]

Bennett IJ, Madden DJ, Vaidya CJ, Howard DV, Howard JH Jr., 2010 Age-related differences in multiple measures of white matter integrity: a diffusion tensor imaging study of healthy aging. Hum. Brain Mapp 31, 378–390. [PubMed: 19662658]

Berman S, West KL, Does MD, Yeatman JD, Mezer AA, 2018 Evaluating g-ratio weighted changes in the corpus callosum as a function of age and sex. Neuroimage 182, 304–313. [PubMed: 28673882]

Bhagat YA, Beaulieu C, 2004 Diffusion anisotropy in subcortical white matter and cortical gray matter: changes with aging and the role of CSF-suppression. J. Magn. Reson. Imag 20, 216–227.

Billiet T, Vandenbulcke M, Madler B, Peeters R, Dhollander T, Zhang H, Deprez S, Van den Bergh BRH, Sunaert S, Emsell L, 2015 Age-related microstructural differences quantified using myelin water imaging and advanced diffusion MRI. Neurobiol. Aging 36, 2107–2121. [PubMed: 25840837]

Branzoli F, Ercan E, Valabregue R, Wood ET, Buijs M, Webb A, Ronen I, 2016 Differentiating between axonal damage and demyelination in healthy aging by combining diffusion-tensor imaging and diffusion-weighted spectroscopy in the human corpus callosum at 7 T. Neurobiol. Aging 47, 210–217. [PubMed: 27616673]

Burcaw LM, Fieremans E, Novikov DS, 2015 Mesoscopic structure of neuronal tracts from time-dependent diffusion. Neuroimage 114, 18–37. [PubMed: 25837598]

Burzynska AZ, Preuschhof C, Backman L, Nyberg L, Li SC, Lindenberger U, Heekeren HR, 2010 Age-related differences in white matter microstructure: region-specific patterns of diffusivity. Neuroimage 49, 2104–2112. [PubMed: 19782758]

Chad JA, Pasternak O, Salat DH, Chen JJ, 2018 Re-examining age-related differences in white matter microstructure with free-water corrected diffusion tensor imaging. Neurobiol. Aging 71, 161–170. [PubMed: 30145396]

Cox SR, Ritchie SJ, Tucker-Drob EM, Liewald DC, Hagenaars SP, Davies G, Wardlaw JM, Gale CR, Bastin ME, Deary IJ, 2016 Ageing and brain white matter structure in 3,513 UK Biobank participants. Nat. Commun 7, 13629. [PubMed: 27976682]

Dale AM, Fischl B, Sereno MI, 1999 Cortical surface-based analysis. I. Segmentation and surface reconstruction. Neuroimage 9, 179–194. [PubMed: 9931268]

Davis SW, Dennis NA, Buchler NG, White LE, Madden DJ, Cabeza R, 2009 Assessing the effects of age on long white matter tracts using diffusion tensor tractography. Neuroimage 46, 530–541. [PubMed: 19385018]

de Lange AG, Brathen AC, Grydeland H, Sexton C, Johansen-Berg H, Andersson JL, Rohani DA, Nyberg L, Fjell AM, Walhovd KB, 2016 White matter integrity as a marker for cognitive plasticity in aging. Neurobiol. Aging 47, 74–82. [PubMed: 27565301]

De Santis S, Jones DK, Roebroeck A, 2016 Including diffusion time dependence in the extra-axonal space improves in vivo estimates of axonal diameter and density in human white matter. Neuroimage 130, 91–103. [PubMed: 26826514]

Draganski B, Ashburner J, Hutton C, Kherif F, Frackowiak RS, Helms G, Weiskopf N, 2011 Regional specificity of MRI contrast parameter changes in normal ageing revealed by voxel-based quantification (VBQ). Neuroimage 55, 1423–1434. [PubMed: 21277375]

Dyrby TB, Sogaard LV, Hall MG, Ptito M, Alexander DC, 2013 Contrast and stability of the axon diameter index from microstructure imaging with diffusion MRI. Magn. Reson. Med 70, 711–721. [PubMed: 23023798]

Fan Q, Nummenmaa A, Wichtmann B, Witzel T, Mekkaoui C, Schneider W, Wald LL, Huang SY, 2018 Validation of diffusion MRI estimates of compartment size and volume fraction in a biomimetic brain phantom using a human MRI scanner with 300mT/m maximum gradient strength. Neuroimage 182, 469–478. [PubMed: 29337276]

Fan Q, Nummenmaa A, Witzel T, Zanzonico R, Keil B, Cauley S, Polimeni JR, Tisdall D, Van Dijk KR, Buckner RL, Wedeen VJ, Rosen BR, Wald LL, 2014 Investigating the capability to resolve complex white matter structures with high b- value diffusion magnetic resonance imaging on the MGH-USC Connectom scanner. Brain Connect 4, 718–726. [PubMed: 25287963]

Fan Q, Witzel T, Nummenmaa A, Van Dijk KR, Van Horn JD, Drews MK, Somerville LH, Sheridan MA, Santillana RM, Snyder J, Hedden T, Shaw EE, Hollinshead MO, Renvall V, Zanzonico R, Keil B, Cauley S, Polimeni JR, Tisdall D, Buckner RL, Wedeen VJ, Wald LL, Toga AW, Rosen BR, 2016 MGH-USC Human Connectome Project datasets with ultra-high b-value diffusion MRI. Neuroimage 124, 1108–1114. [PubMed: 26364861]

Feinberg DA, Moeller S, Smith SM, Auerbach E, Ramanna S, Gunther M, Glasser MF, Miller KL, Ugurbil K, Yacoub E, 2010 Multiplexed echo planar imaging for sub-second whole brain FMRI and fast diffusion imaging. PLoS One 5, e15710. [PubMed: 21187930]

Feinberg DA, Setsompop K, 2013 Ultra-fast MRI of the human brain with simultaneous multi-slice imaging. J. Magn. Reson 229, 90–100. [PubMed: 23473893]

Fieremans E, Burcaw LM, Lee HH, Lemberskiy G, Veraart J, Novikov DS, 2016 In vivo observation and biophysical interpretation of time-dependent diffusion in human white matter. Neuroimage 129, 414–427. [PubMed: 26804782]

Fieremans E, Jensen JH, Helpern JA, 2011 White matter characterization with diffusional kurtosis imaging. Neuroimage 58, 177–188. [PubMed: 21699989]

Fischl B, 2012 FreeSurfer. Neuroimage 62, 774–781. [PubMed: 22248573]

Fischl B, Salat DH, Busa E, Albert M, Dieterich M, Haselgrove C, van der Kouwe A, Killiany R, Kennedy D, Klaveness S, Montillo A, Makris N, Rosen B, Dale AM, 2002 Whole brain segmentation: automated labeling of neuroanatomical structures in the human brain. Neuron 33, 341–355. [PubMed: 11832223]

Fischl B, Sereno MI, Dale AM, 1999 Cortical surface-based analysis. II: inflation, flattening, and a surface-based coordinate system. Neuroimage 9, 195–207. [PubMed: 9931269]

Fischl B, van der Kouwe A, Destrieux C, Halgren E, Segonne F, Salat DH, Busa E, Seidman LJ, Goldstein J, Kennedy D, Caviness V, Makris N, Rosen B, Dale AM, 2004 Automatically parcellating the human cerebral cortex. Cerebr. Cortex 14, 11–22.

Fjell AM, Sneve MH, Grydeland H, Storsve AB, Amlien IK, Yendiki A, Walhovd KB, 2017 Relationship between structural and functional connectivity change across the adult lifespan: a longitudinal investigation. Hum. Brain Mapp 38, 561–573. [PubMed: 27654880]

Fjell AM, Sneve MH, Storsve AB, Grydeland H, Yendiki A, Walhovd KB, 2016 Brain events underlying episodic memory changes in aging: a longitudinal investigation of structural and functional connectivity. Cerebr. Cortex 26, 1272–1286.

Fjell AM, Walhovd KB, Fennema-Notestine C, McEvoy LK, Hagler DJ, Holland D, Brewer JB, Dale AM, 2009 One-year brain atrophy evident in healthy aging. J. Neurosci 29, 15223–15231. [PubMed: 19955375]

Giorgio A, Santelli L, Tomassini V, Bosnell R, Smith S, De Stefano N, Johansen-Berg H, 2010 Age-related changes in grey and white matter structure throughout adulthood. Neuroimage 51, 943–951. [PubMed: 20211265]

Griswold MA, Jakob PM, Heidemann RM, Nittka M, Jellus V, Wang J, Kiefer B, Haase A, 2002 Generalized autocalibrating partially parallel acquisitions (GRAPPA). Magn. Reson. Med 47, 1202–1210. [PubMed: 12111967]

Gunning-Dixon FM, Brickman AM, Cheng JC, Alexopoulos GS, 2009 Aging of cerebral white matter: a review of MRI findings. Int. J. Geriatr. Psychiatry 24, 109–117. [PubMed: 18637641]

Head D, Buckner RL, Shimony JS, Williams LE, Akbudak E, Conturo TE, McAvoy M, Morris JC, Snyder AZ, 2004 Differential vulnerability of anterior white matter in nondemented aging with minimal acceleration in dementia of the Alzheimer type: evidence from diffusion tensor imaging. Cerebr. Cortex 14, 410–423.

Hofer S, Frahm J, 2006 Topography of the human corpus callosum revisited- comprehensive fiber tractography using diffusion tensor magnetic resonance imaging. Neuroimage 32, 989–994. [PubMed: 16854598]

Hsu JL, Leemans A, Bai CH, Lee CH, Tsai YF, Chiu HC, Chen WH, 2008 Gender differences and age-related white matter changes of the human brain: a diffusion tensor imaging study. Neuroimage 39, 566–577. [PubMed: 17951075]

Huang S, Witzel T, Fan Q, McNab JA, Wald LL, Nummenmaa A, 2015a TractCaliber: Axon Diameter Estimation across White Matter Tracts in the in Vivo Human Brain Using 300 mT/m Gradients. Proc ISMRM, Toronto, Canada.

Huang SY, Nummenmaa A, Witzel T, Duval T, Cohen-Adad J, Wald LL, McNab JA, 2015b The impact of gradient strength on in vivo diffusion MRI estimates of axon diameter. Neuroimage 106, 464–472. [PubMed: 25498429]

Huang SY, Tobyne SM, Nummenmaa A, Witzel T, Wald LL, McNab JA, Klawiter EC, 2016 Characterization of axonal disease in patients with multiple Sclerosis using high-gradient-diffusion MR imaging. Radiology 151–582.

Janowsky JS, Kaye JA, Carper RA, 1996 Atrophy of the corpus callosum in Alzheimer's disease versus healthy aging. J. Am. Geriatr. Soc 44, 798–803. [PubMed: 8675927]

Jeeves MA, Moes P, 1996 Interhemispheric transfer time differences related to aging and gender. Neuropsychologia 34, 627–636. [PubMed: 8783215]

Jensen JH, Helpern JA, 2010 MRI quantification of non-Gaussian water diffusion by kurtosis analysis. NMR Biomed 23, 698–710. [PubMed: 20632416]

Keil B, Blau JN, Biber S, Hoecht P, Tountcheva V, Setsompop K, Triantafyllou C, Wald LL, 2013 A 64-channel 3T array coil for accelerated brain MRI. Magn. Reson. Med 70, 248–258. [PubMed: 22851312]

Kemper TL, 1994 Neuroanatomical and Neuropathological Changes during Aging and Dementia. Clinical Neurology of Aging, second ed. Oxford University Press, New York, NY, US, pp. 3–67.

Kennedy KM, Raz N, 2009 Aging white matter and cognition: differential effects of regional variations in diffusion properties on memory, executive functions, and speed. Neuropsychologia 47, 916–927. [PubMed: 19166865]

Kubicki M, Baxi M, Pasternak O, Tang Y, Karmacharya S, Chunga N, Lyall AE, Rathi Y, Eckbo R, Bouix S, Mortazavi F, Papadimitriou G, Shenton ME, Westin CF, Killiany R, Makris N, Rosene DL, 2018 Lifespan trajectories of white matter changes in rhesus monkeys. Cerebr. Cortex bhy056 https://doi-org.ezp-prod1.hul.harvard.edu/10.1093/cercor/bhy056.

Lebel C, Caverhill-Godkewitsch S, Beaulieu C, 2010 Age-related regional variations of the corpus callosum identified by diffusion tensor tractography. Neuroimage 52, 20–31. [PubMed: 20362683]

Lebel C, Gee M, Camicioli R, Wieler M, Martin W, Beaulieu C, 2012 Diffusion tensor imaging of white matter tract evolution over the lifespan. Neuroimage 60, 340–352. [PubMed: 22178809]

Lee HH, Fieremans E, Novikov DS, 2018 What dominates the time dependence of diffusion transverse to axons: intra- or extra-axonal water? Neuroimage 182, 500–510. [PubMed: 29253652]

Liu X, Gao X, Zhang L, Yuan Z, Zhang C, Lu W, Cui D, Zheng F, Qiu J, Xie J, 2018 Age-related changes in fiber tracts in healthy adult brains: a generalized q-sampling and connectometry study. J. Magn. Reson. Imag 48, 369–381.

Madden DJ, Bennett IJ, Burzynska A, Potter GG, Chen NK, Song AW, 2012 Diffusion tensor imaging of cerebral white matter integrity in cognitive aging. Biochim. Biophys. Acta 1822, 386–400. [PubMed: 21871957]

Madden DJ, Whiting WL, Huettel SA, White LE, MacFall JR, Provenzale JM, 2004 Diffusion tensor imaging of adult age differences in cerebral white matter: relation to response time. Neuroimage 21, 1174–1181. [PubMed: 15006684]

Makris N, Papadimitriou GM, van der Kouwe A, Kennedy DN, Hodge SM, Dale AM, Benner T, Wald LL, Wu O, Tuch DS, Caviness VS, Moore TL, Killiany RJ, Moss MB, Rosene DL, 2007 Frontal connections and cognitive changes in normal aging rhesus monkeys: a DTI study. Neurobiol. Aging 28, 1556–1567. [PubMed: 16962214]

Marner L, Nyengaard JR, Tang Y, Pakkenberg B, 2003 Marked loss of myelinated nerve fibers in the human brain with age. J. Comp. Neurol 462, 144–152. [PubMed: 12794739]

Mårtensson J, Lätt J, Åhs F, Fredrikson M, Söderlund H, Schiöth HB, Kok J, Kremer B, van Westen D, Larsson EM, Nilsson M, 2018 Diffusion tensor imaging and tractography of the white matter in normal aging: the rate-of-change differs between segments within tracts. Magn. Reson. Imag 45, 113–119.

McNab JA, Edlow BL, Witzel T, Huang SY, Bhat H, Heberlein K, Feiweier T, Liu K, Keil B, Cohen-Adad J, Tisdall MD, Folkerth RD, Kinney HC, Wald LL, 2013 The Human Connectome Project and beyond: initial applications of 300 mT/m gradients. Neuroimage 80, 234–245. [PubMed: 23711537]

Mollink J, Kleinnijenhuis M, Cappellen van Walsum AV, Sotiropoulos SN, Cottaar M, Mirfin C, Heinrich MP, Jenkinson M, Pallebage-Gamarallage M, Ansorge O, Jbabdi S, Miller KL, 2017 Evaluating fibre orientation dispersion in white matter: comparison of diffusion MRI, histology and polarized light imaging. Neuroimage 157, 561–574. [PubMed: 28602815]

Mori S, Oishi K, Jiang H, Jiang L, Li X, Akhter K, Hua K, Faria AV, Mahmood A, Woods R, Toga AW, Pike GB, Neto PR, Evans A, Zhang J, Huang H, Miller MI, van Zijl P, Mazziotta J, 2008 Stereotaxic white matter atlas based on diffusion tensor imaging in an ICBM template. Neuroimage 40, 570–582. [PubMed: 18255316]

Moseley M, 2002 Diffusion tensor imaging and aging - a review. NMR Biomed 15, 553–560. [PubMed: 12489101]

Nasreddine ZS, Phillips NA, Bedirian V, Charbonneau S, Whitehead V, Collin I, Cummings JL, Chertkow H, 2005 The Montreal Cognitive Assessment, MoCA: a brief screening tool for mild cognitive impairment. J. Am. Geriatr. Soc 53, 695–699. [PubMed: 15817019]

Nilsson M, Alexander DC, 2012 Investigating Tissue Microstructure Using Diffusion MRI: How Does the Resolution Limit of the Axon Diameter Relate to the Maximal Gradient Strength? International Society for Magnetic Resonance in Medicine, Melbourne, Australia, p. 3567.

Nilsson M, Lasic S, Drobnjak I, Topgaard D, Westin CF, 2017 Resolution limit of cylinder diameter estimation by diffusion MRI: the impact of gradient waveform and orientation dispersion. NMR Biomed 30.

Novikov DS, Jensen JH, Helpern JA, Fieremans E, 2014 Revealing mesoscopic structural universality with diffusion. Proc. Natl. Acad. Sci. U. S. A 111, 5088–5093. [PubMed: 24706873]

Nusbaum AO, Tang CY, Buchsbaum MS, Wei TC, Atlas SW, 2001 Regional and global changes in cerebral diffusion with normal aging. AJNR Am. J. Neuroradiol 22, 136–142. [PubMed: 11158899]

O'Sullivan M, Jones DK, Summers PE, Morris RG, Williams SC, Markus HS, 2001 Evidence for cortical "disconnection" as a mechanism of age-related cognitive decline. Neurology 57, 632–638. [PubMed: 11524471]

Ota M, Obata T, Akine Y, Ito H, Ikehira H, Asada T, Suhara T, 2006 Age-related degeneration of corpus callosum measured with diffusion tensor imaging. Neuroimage 31, 1445–1452. [PubMed: 16563802]

Pfefferbaum A, Adalsteinsson E, Sullivan EV, 2005 Frontal circuitry degradation marks healthy adult aging: evidence from diffusion tensor imaging. Neuroimage 26, 891–899. [PubMed: 15955499]

Pfefferbaum A, Sullivan EV, 2003 Increased brain white matter diffusivity in normal adult aging: relationship to anisotropy and partial voluming. Magn. Reson. Med 49, 953–961. [PubMed: 12704779]

Pfefferbaum A, Sullivan EV, Hedehus M, Lim KO, Adalsteinsson E, Moseley M, 2000 Age-related decline in brain white matter anisotropy measured with spatially corrected echo-planar diffusion tensor imaging. Magn. Reson. Med 44, 259–268. [PubMed: 10918325]

Raz N, Gunning-Dixon F, Head D, Rodrigue KM, Williamson A, Acker JD, 2004 Aging, sexual dimorphism, and hemispheric asymmetry of the cerebral cortex: replicability of regional differences in volume. Neurobiol. Aging 25, 377–396. [PubMed: 15123343]

Reuter-Lorenz PA, Stanczak L, 2000 Differential effects of aging on the functions of the corpus callosum. Dev. Neuropsychol 18, 113–137. [PubMed: 11143802]

Rojkova K, Volle E, Urbanski M, Humbert F, Dell'Acqua F, Thiebaut de Schotten M, 2016 Atlasing the frontal lobe connections and their variability due to age and education: a spherical deconvolution tractography study. Brain Struct. Funct 221, 1751–1766. [PubMed: 25682261]

Sala S, Agosta F, Pagani E, Copetti M, Comi G, Filippi M, 2012 Microstructural changes and atrophy in brain white matter tracts with aging. Neurobiol. Aging 33, 488–498 e482. [PubMed: 20594616]

Salat DH, Tuch DS, Hevelone ND, Fischl B, Corkin S, Rosas HD, Dale AM, 2005 Age-related changes in prefrontal white matter measured by diffusion tensor imaging. Ann. N. Y. Acad. Sci 1064, 37–49. [PubMed: 16394146]

Schulte T, Sullivan EV, Muller-Oehring EM, Adalsteinsson E, Pfefferbaum A, 2005 Corpus callosal microstructural integrity influences interhemispheric processing: a diffusion tensor imaging study. Cerebr. Cortex 15, 1384–1392.

Serbruyns L, Gooijers J, Caeyenberghs K, Meesen RL, Cuypers K, Sisti HM, Leemans A, Swinnen SP, 2015 Bimanual motor deficits in older adults predicted by diffusion tensor imaging metrics of corpus callosum subregions. Brain Struct. Funct 220, 273–290. [PubMed: 24158531]

Setsompop K, Cohen-Adad J, Gagoski BA, Raij T, Yendiki A, Keil B, Wedeen VJ, Wald LL, 2012a Improving diffusion MRI using simultaneous multi-slice echo planar imaging. Neuroimage 63, 569–580. [PubMed: 22732564]

Setsompop K, Gagoski BA, Polimeni JR, Witzel T, Wedeen VJ, Wald LL, 2012b Blipped-controlled aliasing in parallel imaging for simultaneous multislice echo planar imaging with reduced g-factor penalty. Magn. Reson. Med 67, 1210–1224. [PubMed: 21858868]

Setsompop K, Kimmlingen R, Eberlein E, Witzel T, Cohen-Adad J, McNab JA, Keil B, Tisdall MD, Hoecht P, Dietz P, Cauley SF, Tountcheva V, Matschl V, Lenz VH, Heberlein K, Potthast A, Thein H, Van Horn J, Toga A, Schmitt F, Lehne D, Rosen BR, Wedeen V, Wald LL, 2013 Pushing the limits of in vivo diffusion MRI for the human connectome project. Neuroimage 80, 220–233. [PubMed: 23707579]

Sexton CE, Walhovd KB, Storsve AB, Tamnes CK, Westlye LT, Johansen-Berg H, Fjell AM, 2014 Accelerated changes in white matter microstructure during aging: a longitudinal diffusion tensor imaging study. J. Neurosci 34, 15425–15436. [PubMed: 25392509]

Smith SM, Jenkinson M, Woolrich MW, Beckmann CF, Behrens TE, Johansen-Berg H, Bannister PR, De Luca M, Drobnjak I, Flitney DE, Niazy RK, Saunders J, Vickers J, Zhang Y, De Stefano N, Brady JM, Matthews PM, 2004 Advances in functional and structural MR image analysis and implementation as FSL. Neuroimage 23 (Suppl. 1), S208–S219. [PubMed: 15501092]

Storsve AB, Fjell AM, Yendiki A, Walhovd KB, 2016 Longitudinal changes in white matter tract integrity across the adult lifespan and its relation to cortical thinning. PLoS One 11, e0156770. [PubMed: 27253393]

Stricker NH, Salat DH, Kuhn TP, Foley JM, Price JS, Westlye LT, Esterman MS, McGlinchey RE, Milberg WP, Leritz EC, 2015 Mild cognitive impairment is associated with white matter integrity changes in late-myelinating regions within the corpus callosum. Am. J. Alzheimer's Dis. Other Dementias 31, 68–75.

Sullivan EV, Adalsteinsson E, Hedehus M, Ju C, Moseley M, Lim KO, Pfefferbaum A, 2001 Equivalent disruption of regional white matter microstructure in ageing healthy men and women. Neuroreport 12, 99–104. [PubMed: 11201100]

Sullivan EV, Adalsteinsson E, Pfefferbaum A, 2006 Selective age-related degradation of anterior callosal fiberbundles quantified invivowith fiber tracking. Cerebr. Cortex 16, 1030–1039.

Sullivan EV, Pfefferbaum A, 2006 Diffusion tensor imaging and aging. Neurosci. Biobehav. Rev 30, 749–761. [PubMed: 16887187]

Sullivan EV, Rohlfing T, Pfefferbaum A, 2010 Quantitative fiber tracking of lateral and interhemispheric white matter systems in normal aging: relations to timed performance. Neurobiol. Aging 31, 464–481. [PubMed: 18495300]

Tobyne SM, Boratyn D, Johnson JA, Greve DN, Mainero C, Klawiter EC, 2016 A surface-based technique for mapping homotopic interhemispheric connectivity: development, characterization, and clinical application. Hum. Brain Mapp 37, 2849–2868. [PubMed: 27219660]

Tuch DS, 2004 Q-ball imaging. Magn. Reson. Med 52, 1358–1372. [PubMed: 15562495]

van der Knaap LJ, van der Ham IJM, 2011 How does the corpus callosum mediate interhemispheric transfer? A review. Behav. Brain Res 223, 211–221. [PubMed: 21530590]

van der Kouwe AJ, Benner T, Salat DH, Fischl B, 2008 Brain morphometry with multiecho MPRAGE. Neuroimage 40, 559–569. [PubMed: 18242102]

van Gelderen P, DesPres D, van Zijl PC, Moonen CT, 1994 Evaluation of restricted diffusion in cylinders. Phosphocreatine in rabbit leg muscle. J. Magn. Reson. B 103, 255–260. [PubMed: 8019777]

Vik A, Hodneland E, Haasz J, Ystad M, Lundervold AJ, Lundervold A, 2015 Fractional anisotropy shows differential reduction in frontal-subcortical fiber bundles—a longitudinal MRI study of 76 middle-aged and older adults. Front. Aging Neurosci 7.

Wang D, Chen YJ, Li YH, 2018 Application of super-resolution track-density technique: earlier detection of aging-related subtle alterations than morphological changes in corpus callosum from normal population? J. Magn. Reson. Imag 49, 164–175.

Xie S, Zhang Z, Chang F, Wang Y, Zhang Z, Zhou Z, Guo H, 2016 Subcortical white matter changes with normal aging detected by multi-shot high resolution diffusion tensor imaging. PLoS One 11, e0157533. [PubMed: 27332713]

Yeatman JD, Wandell BA, Mezer AA, 2014 Lifespan maturation and degeneration of human brain white matter. Nat. Commun 5, 4932. [PubMed: 25230200]

Yeh FC, Wedeen VJ, Tseng WY, 2010 Generalized q-sampling imaging. IEEE Trans. Med. Imaging 29, 1626–1635. [PubMed: 20304721]

Zhang H, Schneider T, Wheeler-Kingshott CA, Alexander DC, 2012 NODDI: practical in vivo neurite orientation dispersion and density imaging of the human brain. Neuroimage 61, 1000–1016. [PubMed: 22484410]

Zhang Y, Du AT, Hayasaka S, Jahng GH, Hlavin J, Zhan W, Weiner MW, Schuff N, 2010 Patterns of age-related water diffusion changes in human brain by concordance and discordance analysis. Neurobiol. Aging 31, 1991–2001. [PubMed: 19036473]

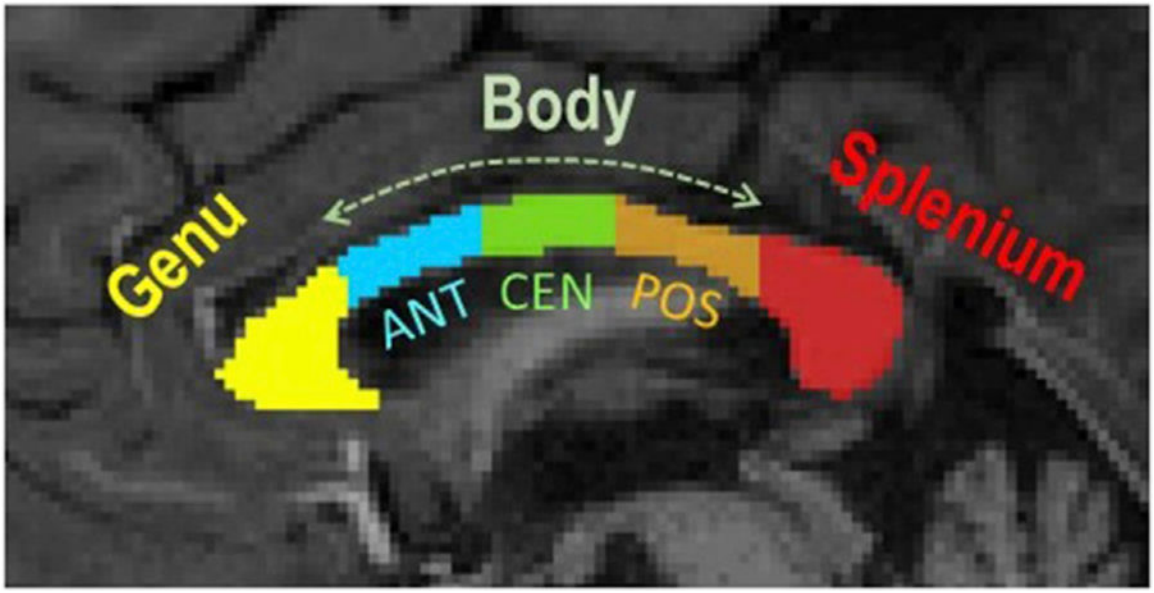

Fig. 1. Corpus callosum ROIs.

Illustration of the corpus callosum segments defined on a mid-sagittal image in a young adult. The axonal metrics and FA were sampled in the whole corpus callosum as well as within five separate ROIs obtained from the Freesurfer automatic segmentation of the corpus callosum. ANT: Anterior; CEN: Central; POS: Posterior.

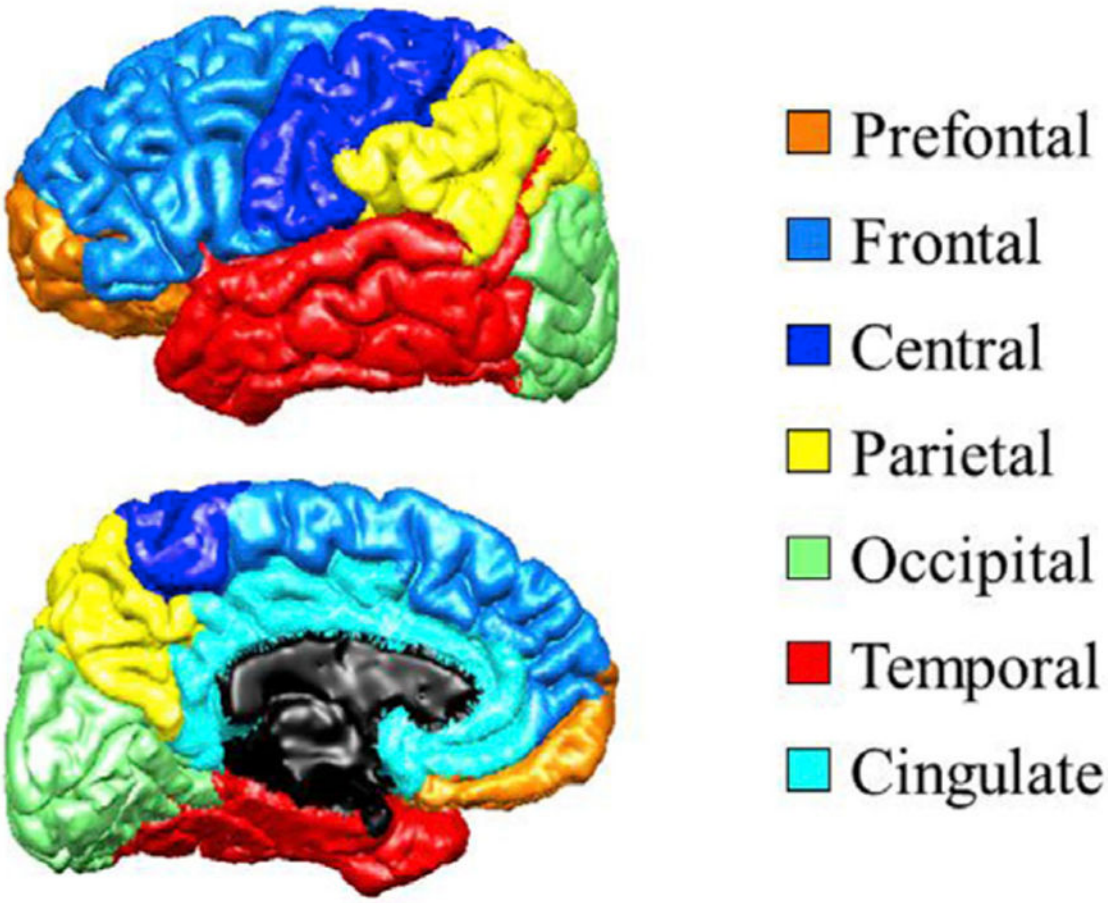

Fig. 2.
Illustration of the cortical segmentation. The cortex was divided into seven lobules using FreeSurfer automatic labeling by regrouping the smaller cortical segments in the Destrieux atlas.

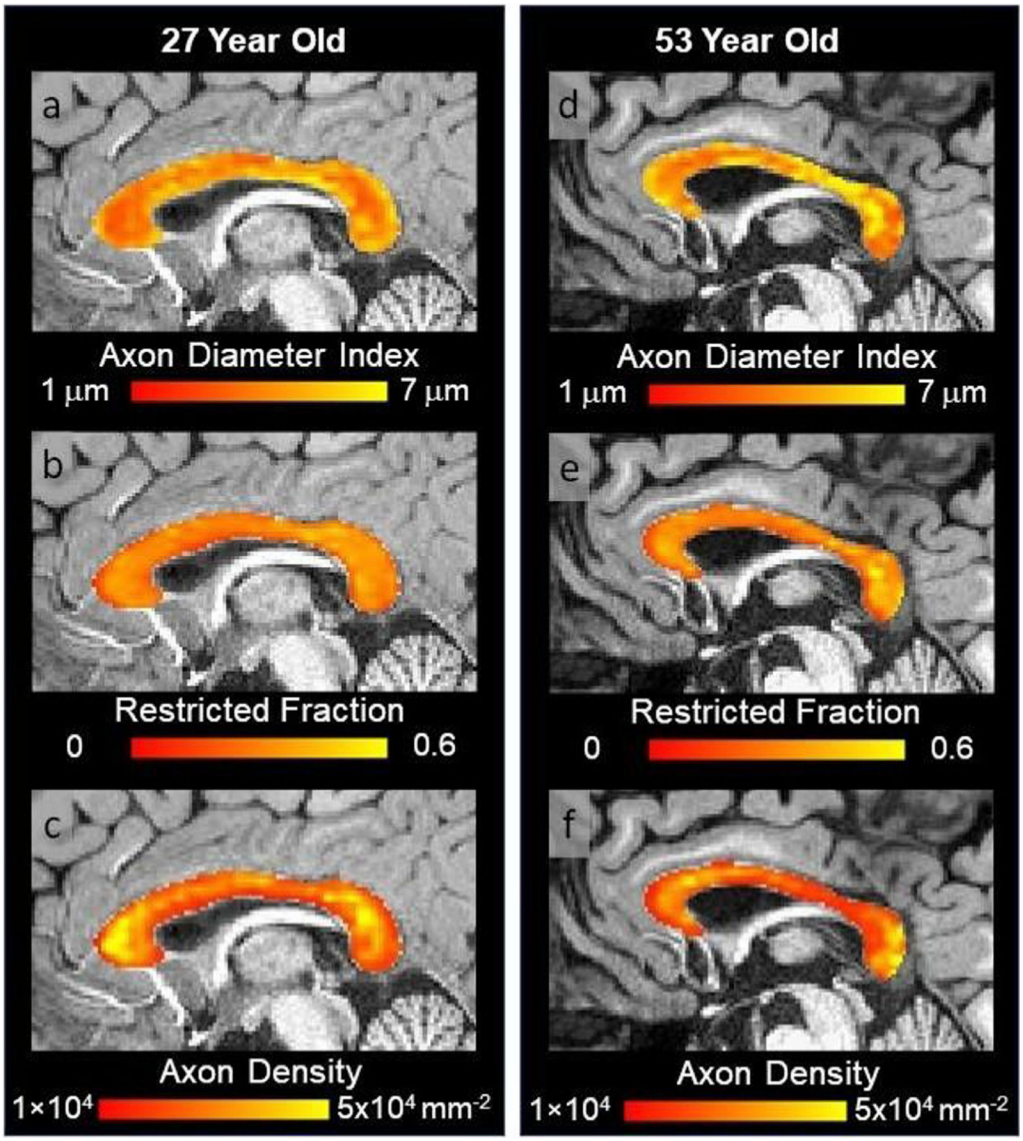

Fig. 3.

Exemplary maps of axon diameter index, restricted volume fraction, and packing density in a healthy young adult (female, 27 years old, a-c) and a healthy older adult (male, 53 years old, d-f). In all subjects, a general trend of smaller axon diameter index and higher packing density in the genu and splenium of the corpus callosum compared to the posterior body was observed. The axon diameter index appeared relatively larger, and the packing density appeared generally reduced throughout the corpus callosum in the older adult participants, while the restricted volume fraction was relatively similar in younger and older adults.

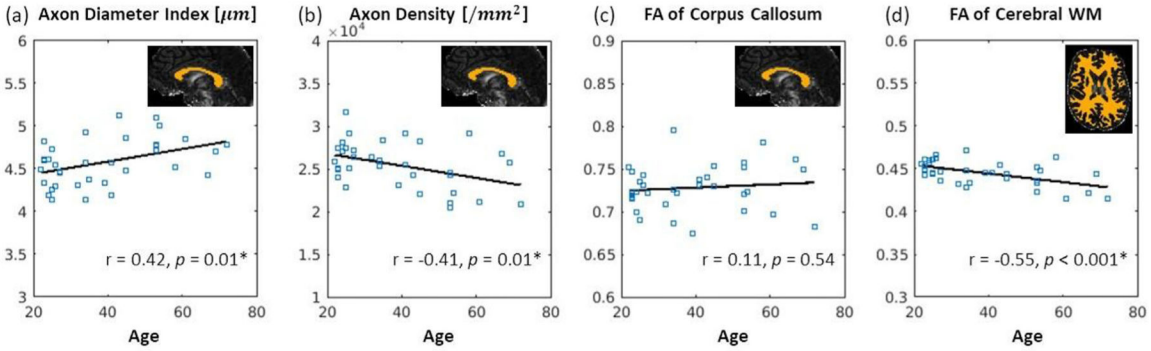

Fig. 4.

Correlations of diffusion metrics in the whole corpus callosum and cerebral white matter with age. (a) Axon diameter index increased with age, and (b) axon density decreased with age. (c) No significant correlation was found between FA and age in the corpus callosum. (d) FA of the cerebral white matter (WM) decreased with age. Pearson's linear correlation was used to report the correlation coefficients (*r*). Raw uncorrected *p*-values are reported, with *p*-values surviving multiple comparisons correction at an FDR threshold of 0.05 denoted with an asterisk (*).

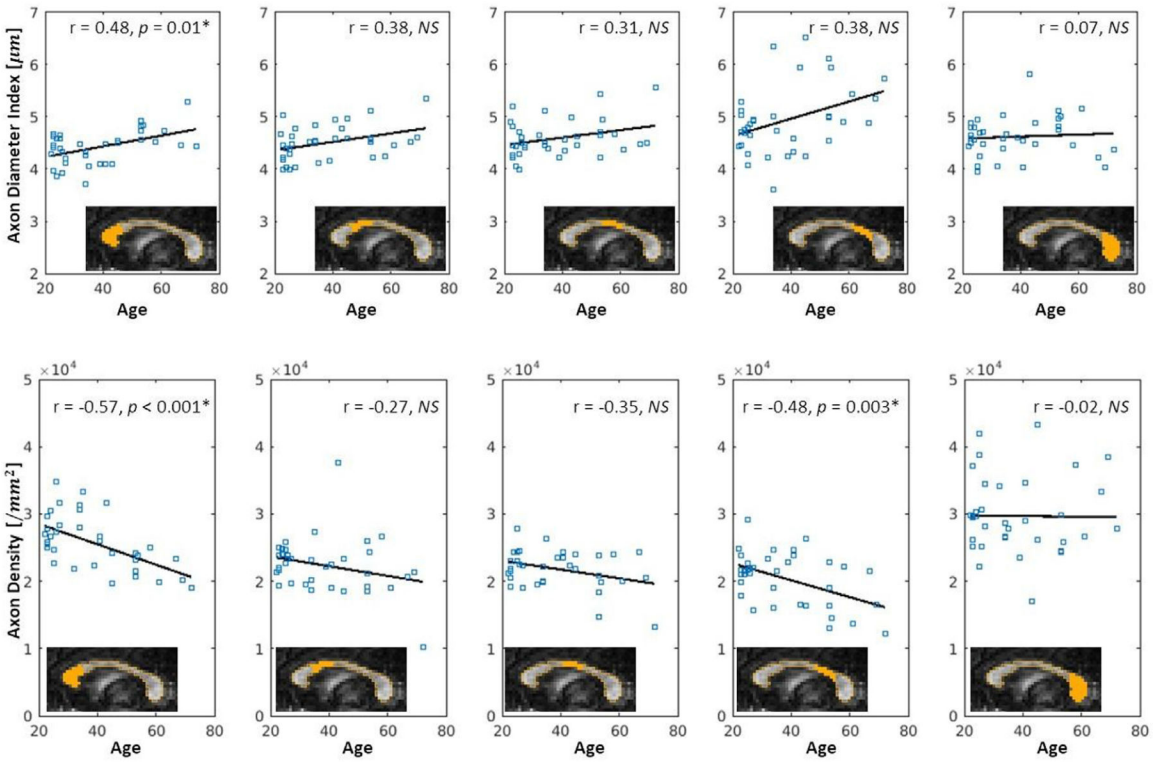

Fig. 5.

Correlation of axon diameter index and axon density with age in the five segments of the corpus callosum defined in Fig. 1. (Top) Overall, axon diameter index increased with age, with the strongest correlation found in the genu of the corpus callosum. (Bottom) Axon density decreased with age throughout the corpus callosum, with the correlations reaching the level of significance in the genu and posterior body. No significant correlation was found between axon diameter index or axon density with age in the splenium. Raw uncorrected *p*-values are reported, with *p*-values surviving multiple comparisons correction at an FDR threshold of 0.05 denoted with an asterisk (*). NS: Not significant.

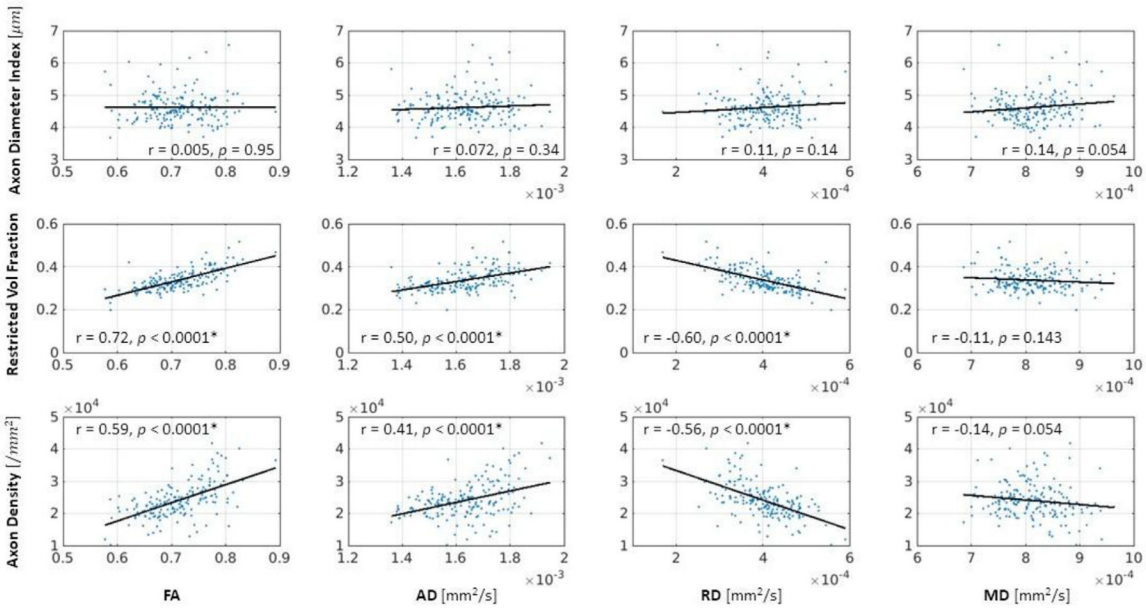

Fig. 6.

Correlation of DTI metrics and axon diameter index, restricted volume fraction, and axon density across all five segments of the corpus callosum. The scatterplots were generated by pooling together all voxels in the corpus callosum of all subjects. No significant correlation was observed between axon diameter index and DTI metrics including FA, AD and RD. On the other hand, a strong positive correlation was identified between restricted volume fraction and FA and RD, and a moderate correlation was appreciated between axon density and DTI metrics. Raw uncorrected *p*-values are reported, with *p*-values surviving multiple comparisons correction at an FDR threshold of 0.05 denoted with an asterisk (*).

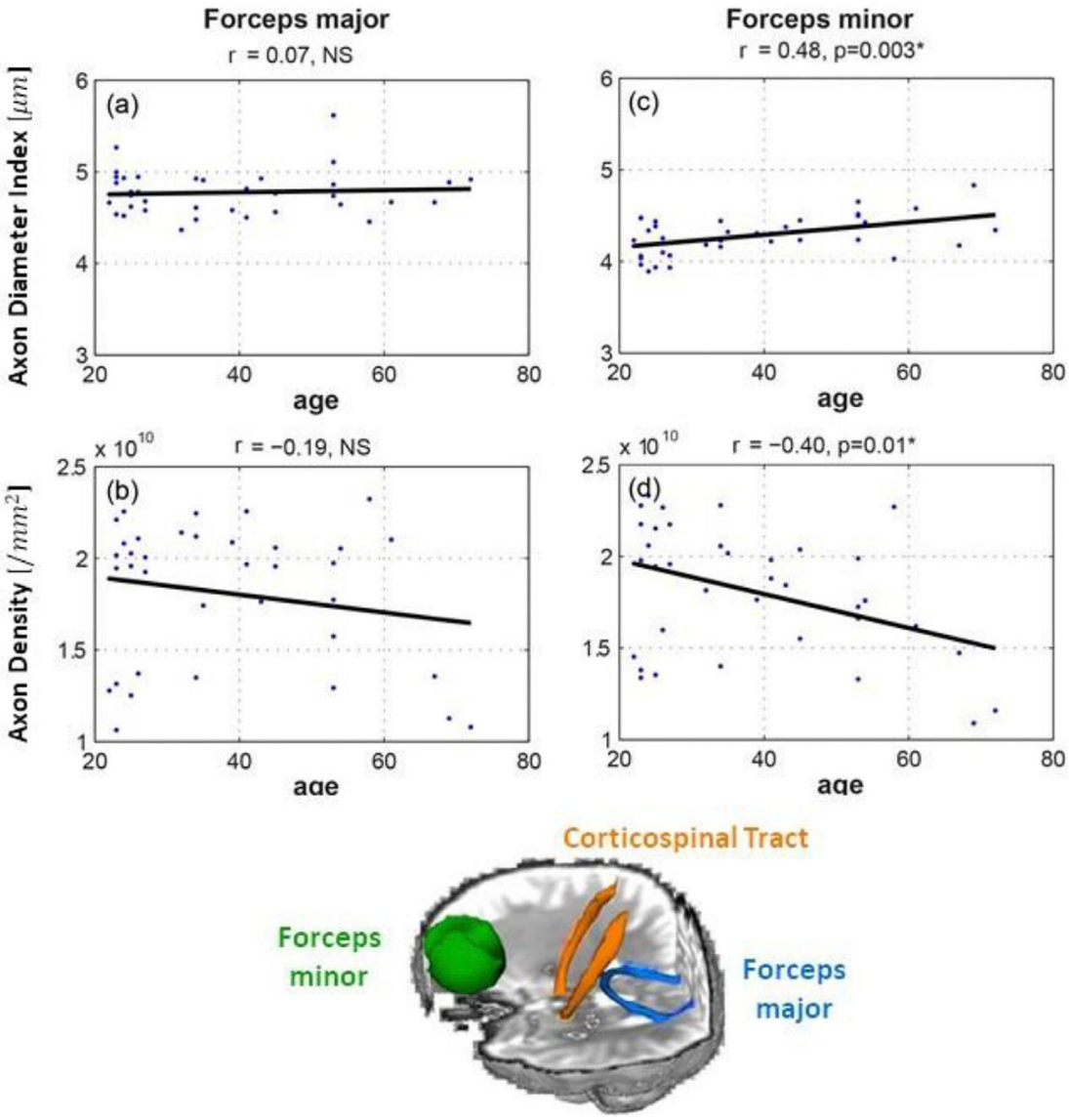

Fig. 7.

Correlation of axon diameter index and axon density with age in the forceps major and forceps minor. of the corpus callosum defined in Fig. 1. Axon diameter index increased and axon density decreased with increasing age in the forceps minor. By comparison, in the forceps major, no significant correlation was seen between age and axon diameter index or axon density. Raw uncorrected *p*-values are reported, with *p*-values surviving multiple comparisons correction at an FDR threshold of 0.05 denoted with an asterisk (*). NS: Not significant.

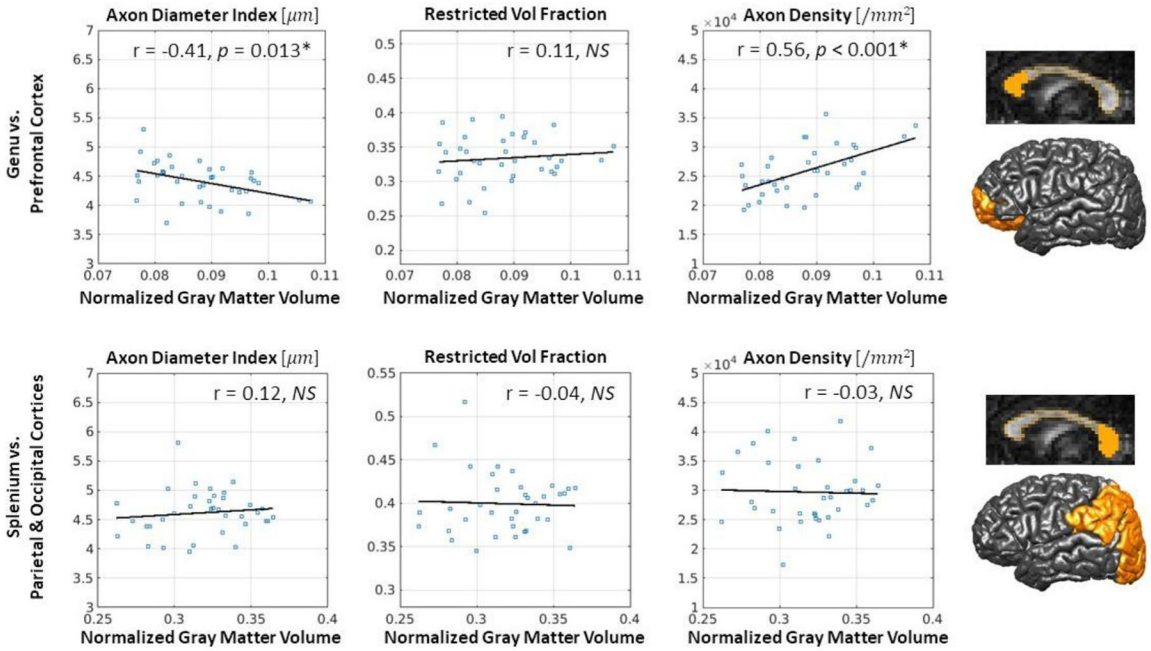

Fig. 8.

Correlation of the axonal metrics in the genu (top) and splenium (bottom) of the corpus callosum with the gray matter volumes of their primary associated cortical regions. Raw uncorrected *p*-values are reported, with p-values surviving multiple comparisons correction at an FDR threshold of 0.05 denoted with an asterisk (*). NS: Not significant.

Table 1

Diffusion MRI parameters.

Δ (ms)	δ (ms)	*b*-values (s/mm^2)	# of gradient directions
19	8	50, 350, 800, 1500	32
	8	2400, 3450, 4750, 6000	64
49	8	200, 950, 2300	32
	8	4250, 6750, 9850, 13500, 17800	64

Table 2

Partial correlation coefficients of imaging metrics with age adjusted for gender. Raw uncorrected *p*-values are reported, with *p*-values surviving multiple comparisons correction at an FDR threshold of 0.05 denoted with an asterisk (*)

	Correlation Coefficients	***p*-value**
Axon diameter index	0.42	0.01*
Restricted Volume Fraction	0.08	0.647
Packing Density	−0.41	0.01*
Whole Corpus Callosum FA	0.11	0.522
Cerebral White Matter FA	−0.55	<0.001*
Corpus Callosum Area	−0.52	0.001*
Normalized Corpus Callosum Area	−0.45	0.007*